

Nonequilibrium dual-boson approach

Feng Chen,^{1,*} Mikhail I. Katsnelson,^{2,†} and Michael Galperin^{3,‡}

¹*Department of Physics, University of California San Diego, La Jolla, CA 92093, USA*

²*Radboud University Nijmegen, Institute for Molecules and Materials, 6525AJ Nijmegen, The Netherlands*

³*Department of Chemistry & Biochemistry, University of California San Diego, La Jolla, CA 92093, USA*

We develop nonequilibrium auxiliary quantum master equation dual boson method (aux-DB), and argue that it presents a convenient way to describe steady states of correlated impurity models (such as single molecule optoelectronic devices) where electron and energy transport should be taken into account. The aux-DB is shown to provide high accuracy with relatively low numerical cost. Theoretical analysis is followed by illustrative simulations within generic junction models, where the new scheme is benchmarked against numerically exact results.

I. INTRODUCTION

Fast development of nano-fabrication techniques combined with advances in laser technology lead to tremendous progress in optical studies of nanoscale systems. Optical spectroscopy of single molecules in current carrying junctions became reality. Surface¹⁻³ and tip⁴⁻⁶ enhanced Raman spectroscopies (SERS and TERS) as well as bias-induced electroluminescence⁷⁻¹³ measurements yield information on extent of heating of vibrational and electronic degrees of freedom in biased junctions, electron transport noise characteristics, molecular structure, dynamics and chemistry. Combination of molecular electronics with nonlinear optical spectroscopy resulted in emergence of a new field of research coined optoelectronics^{14,15}.

Optical response of single molecule junctions is only possible due to strong enhancement of the signal by surface plasmons¹⁶. Large fields and confinement result in strong interaction between molecular and plasmonic excitations. Note also recent experiments on ultra-strong light-matter interaction in single molecule nano-cavities (at the moment, in the absence of electron current)^{17,18}. At nanoscale classical electrodynamics becomes inadequate as it cannot describe quantum coherence and mixing between plasmon and molecular exciton, while strong interactions require to go beyond perturbation theory.

Development of theoretical methods for simulation of strongly correlated open nonequilibrium impurity systems is a prerequisite in modeling nanoscale molecular devices with potential applications from optical characterization and control to energy harvesting, spintronics, and quantum computation. With numerically exact techniques, such as continuous time quantum Monte Carlo¹⁹⁻²¹ or renormalization group methods²²⁻²⁵, being computationally costly and thus mostly focused on simple models, relatively numerically inexpensive and sufficiently accurate schemes for realistic simulations are in high demand.

One of such perspective universal impurity solvers is the nonequilibrium dual fermion (DF) approach originally introduced in Ref. 26. Recently, the approach was modified²⁷ to reduce computational cost and improve ability to simulate steady-states of correlated impurity

models. Note that focus of the dual fermion approach is electron transport. At the same time, simulations of optoelectronic devices require accounting also for energy transfer.

Here, we introduce *auxiliary quantum master equation (QME) - nonequilibrium dual boson (aux-DB) method* - a universal nonequilibrium impurity solver which accounts for both charge and energy transport in strongly correlated open systems. Similar to DF of Ref. 26 being nonequilibrium version of the equilibrium DF method²⁸⁻³¹ (DF inspired superperturbation theory), aux-DB has its origin in equilibrium DB approach³²⁻³⁹. Below, after introducing nonequilibrium DB in Section II, in Section III we present auxiliary quantum master equation (QME) treatment within the method. Theoretical considerations are followed by illustrative numerical simulations within generic junction models in Section IV. Section V concludes.

II. NONEQUILIBRIUM DB THEORY

Here we present a short description of the aux-DB method. Detailed derivations are given in Appendix A. Similar to the DF method, in the nonequilibrium DB approach one considers reduced dynamics of an open quantum system with interactions confined to the molecular subspace. Contrary to the DF method, in addition to contacts (Fermi baths) the system is coupled also to Bose

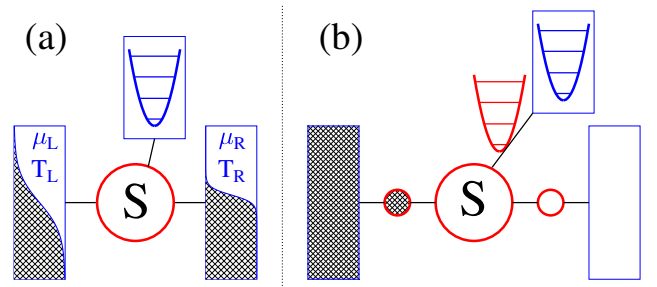


FIG. 1: Nonequilibrium junction model. Shown are (a) Physical model and (b) Reference system within aux-DB approach.

bath(s). Effect of the baths enters the effective action defined on the Keldysh contour⁴⁰ via corresponding self-energies Σ (for Fermi baths) and Π (for Bose baths)

$$S[\bar{d}, d] = \bar{d}_1 [G_0^{-1} - \Sigma^B]_{12} d_2 - \bar{b}_1 \Pi_{1,2}^B b_2 + S^{int}[\bar{d}, d] \quad (1)$$

Here and below summation of repeating indices is assumed. In (1) $\bar{d}_i \equiv d_{m_i}(\tau_i)$ ($d_i \equiv d_{m_i}(\tau_i)$) is the Grassmann variable corresponding to creation (annihilation) operator $\hat{d}_{m_i}^\dagger(\tau_i)$ ($\hat{d}_{m_i}(\tau_i)$) represents both molecular (spin-)orbital m_i and contour variable τ_i , of an electron in orbital m_i in the Heisenberg picture⁴¹. $b_i = b_{m_i^i m_2^i}(\tau_i) \equiv \bar{d}_{m_i^i}(\tau_i) d_{m_2^i}(\tau_i)$ is the molecular excitation representing optical transition within the molecule from orbital m_2^i to orbital m_1^i at contour variable τ_i . Sum over indices includes summation over molecular orbitals (optical transitions) and contour integration: $\sum_i \dots \equiv \sum_{m_i} \int_c d\tau_i \dots (\sum_{m_1^i, m_2^i} \int_c d\tau_i \dots)$. G_0^{-1} is the inverse free Green's function (GF)⁴²

$$[G_0^{-1}]_{12} \equiv \delta(\tau_1, \tau_2) [i\partial_{\tau_1} \delta_{m_1, m_2} - H_{m_1 m_2}^0(\tau_1)] - \Sigma_{12}^{irr}, \quad (2)$$

Σ^B and Π^B are respectively self-energies due to coupling to Fermi (contacts) and Bose (plasmon) baths,

$$\begin{aligned} \Sigma_{m_1 m_2}^B(\tau_1, \tau_2) &= V_{m_1 k} g_k(\tau_1, \tau_2) V_{k m_2} \quad \text{and} \\ \Pi_{m_1 m_2, m_3 m_4}^B(\tau_1, \tau_2) &= V_{m_1 m_2, \alpha} d_\alpha(\tau_1, \tau_2) V_{\alpha, m_3 m_4}. \end{aligned} \quad (3)$$

In Eqs. (2)-(3), $H_{m_1 m_2}^0(\tau)$ is the non-interacting part of the molecular Hamiltonian, $\Sigma_{m_1 m_2}^{irr}(\tau_1, \tau_2) \sim \delta(\tau_1, \tau_2)$ is the irregular self-energy, V_{mk} and $V_{m_1 m_2, \alpha}$ are matrix elements for electron transfer from contact state k to molecular orbital m and for optical electron transfer from orbital m_1 to m_2 with absorption of phonon in mode α , respectively. $g_k(\tau_1, \tau_2) \equiv -i\langle T_c \hat{c}_k(\tau_1) \hat{c}_k^\dagger(\tau_2) \rangle$ and $d_\alpha(\tau_1, \tau_2) \equiv -i\langle T_c \hat{a}_\alpha(\tau_1) \hat{a}_\alpha^\dagger(\tau_2) \rangle$ are GFs of free electron in state k of the contacts and free phonon in mode α . All intra-molecular interactions are within the (unspecified) contribution to the action $S^{int}[\bar{d}, d]$.

As in equilibrium DB³³, one introduces an exactly solvable *reference system* (see below). Similarly to aux-DF²⁷, the true baths are approximated by a finite number of auxiliary discrete modes subject to Lindbladian evolution (see Fig. 1b). Thus, action of the reference system $\tilde{S}[\bar{d}, d]$ is known and has the same general form (1) with true self-energies Σ^B and Π^B substituted by their approximate representations $\tilde{\Sigma}^B$ and $\tilde{\Pi}^B$. The desired action S can then be written as

$$S[\bar{d}, d] = \tilde{S}[\bar{d}, d] + \bar{d}_1 \delta\Sigma_{12}^B d_2 + \bar{b}_1 \delta\Pi_{12}^B b_2. \quad (4)$$

where $\delta\Sigma^B \equiv \tilde{\Sigma}^B - \Sigma^B$ and $\delta\Pi^B \equiv \tilde{\Pi}^B - \Pi^B$.

Because direct application of standard diagrammatic expansion around the interacting reference system is not possible (the Wick's theorem does not apply⁴³), two artificial particles, *dual fermion* (f) and *dual boson* (η), are introduced which is used to unravel last two terms in

(4) via the Hubbard-Stratonovich transformation⁴⁴. Integrating out molecular fermions (d and \bar{d}) and comparing the fourth order cumulant expansion of the resulting expression with the general form of action for dual particles,

$$\begin{aligned} S^D[f^*, f] &= \bar{f}_1 [(G_0^{DF})^{-1} - \Sigma^{DF}]_{12} f_2 \\ &+ \bar{\eta}_1 [(D_0^{DB})^{-1} - \Pi^{DB}]_{12} \eta_2, \end{aligned} \quad (5)$$

one gets

$$\begin{aligned} (G_0^{DF})_{12}^{-1} &= -g_{12}^{-1} - g_{13}^{-1} [\delta\Sigma^B]_{34}^{-1} g_{42}^{-1}, \\ (D_0^{DB})_{12}^{-1} &= -\chi_{12}^{-1} - \chi_{13}^{-1} [\delta\Pi^B]_{34}^{-1} \chi_{42}^{-1}, \\ \Sigma_{12}^{DF} &= \left(\Gamma_{13;42} + i(\gamma_{514} \delta_{326} - \gamma_{512} \delta_{346} \right. \\ &\quad \left. + \gamma_{532} \delta_{146} - \gamma_{534} \delta_{126}) [D_0^{DB}]_{65} \right) [G_0^{DF}]_{43} \\ &\quad - \left(\langle \hat{b}_5^\dagger \rangle \chi_{54}^{-1} \gamma_{312} + \chi_{35}^{-1} \langle \hat{b}_5 \rangle \delta_{124} \right) [D_0^{DB}]_{43} \\ \Pi_{12}^{DB} &= -i\gamma_{145} \delta_{632} [G_0^{DF}]_{34} [G_0^{DF}]_{56} \end{aligned} \quad (6)$$

Here g_{12} and χ_{12} are single particle GFs of fermion and molecular excitation of the reference system, γ_{123} , δ_{123} and $\Gamma_{13;24}$ are vertices⁴⁵ (see Eq. (A12) and Fig. 5 in Appendix A).

With dual particles GFs,

$$\begin{aligned} (G^{DF}) &= [(G_0^{DF})^{-1} - \Sigma^{DF}]^{-1} \quad \text{and} \\ (D^{DB}) &= [(D_0^{DB})^{-1} - \Pi^{DB}]^{-1}, \end{aligned} \quad (7)$$

known, the single-particle (G) and two-particle (D) GFs of the molecule are obtained from

$$\begin{aligned} G &= (\delta\Sigma^B)^{-1} + [g \delta\Sigma^B]^{-1} G^{DF} [\delta\Sigma^B g]^{-1} \\ D &= (\delta\Pi^B)^{-1} + [\chi \delta\Pi^B]^{-1} D^{DF} [\delta\Pi^B \chi]^{-1} \end{aligned} \quad (8)$$

Note, here the two-particle GF is correlation function of molecular optical excitation operators. G yields information on orbital populations, spectral functions and electron current in the junction, while D is used in calculation of boson (phonon) flux.

III. REFERENCE SYSTEM

Construction of a reference system to a large extent relies on accurate reproduction of the physical system's hybridization functions Σ^B and Π^B . Accurate choice of the reference system parameters was recently discussed in Refs. 46,47 for Bose baths and in Refs. 48–51 for Fermi baths. Here we combine both considerations by introducing as the reference system physical system complemented with a finite number of auxiliary unitary modes (A) subject to Lindbladian evolution. This includes finite number of sites representing Fermi baths and modes

representing Bose bath (see Fig. 1b and Appendix B). Dynamics of the extended SA system (molecule plus finite number of sites and modes) is driven by Markov Lindblad-type evolution

$$\frac{d\rho^{SA}(t)}{dt} = -i\mathcal{L}\rho^{SA}(t). \quad (9)$$

Here, $\rho^{SA}(t)$ is the extended system density operator and \mathcal{L} is the Liouvillian. Note that Refs. 46 and 51 prove that, in principle, Markov dynamics of the extended system can exactly reproduce non-Markov unitary dynamics of the physical system S as long as free correlation function of the auxiliary modes accurately reproduces the correlation function of the full baths. However, in realistic calculations this representation is approximate due to restriction on number of auxiliary sites and modes which can be taken in consideration. Thus, the aux-DB accounting for the difference between true and reference system hybridization functions, Eq. (6), is very useful in correcting the approximate mapping.

The aux-DB approach, Eqs. (5)-(8), requires single- and two-particle GFs g and χ and vertices Γ , γ and δ of the reference system as an input. Those are obtained by solving the QME (9) and employing the quantum regression relation (see Appendix C for details).

Below we focus on steady state and consider a reference system of size small enough that exact diagonalization can be employed. For larger systems more advanced methods (e.g. matrix product states⁴⁹) may be used. We note that while MPS is only works for 1d problems, this does not impose limitation on the dimensionality of original (physical) problem, because any number and geometry of couplings in the physical problem can be mapped onto effectively 1d formulation in auxiliary reference system with only two (for Fermi) or one (for Bose) baths.

IV. NUMERICAL RESULTS AND DISCUSSION

Here we illustrate the aux-DB method with numerical simulations within generic junction models: resonant level model (RLM) and Anderson impurity model (AIM) coupled to Fermi and Bose baths.

A. Model

We apply the aux-DB method to generic models with junction constructed from a system S coupled to two Fermi (L and R) and one Boson bath (P) (see Fig. 1a). The Hamiltonian is

$$\hat{H} = \hat{H}_S + \sum_{B=L,R,P} (\hat{H}_B + \hat{V}_{SB}), \quad (10)$$

where

$$\begin{aligned} \hat{H}_{L(R)} &= \sum_{k \in L(R)} \varepsilon_k \hat{c}_k^\dagger \hat{c}_k \\ \hat{H}_P &= \sum_{\alpha \in P} \omega_\alpha \hat{a}_\alpha^\dagger \hat{a}_\alpha \end{aligned} \quad (11)$$

are Hamiltonians of the contact L (R) and phonon bath P .

$$\begin{aligned} \hat{V}_{SL(R)} &= \sum_m \sum_{k \in L(R)} (V_{mk} \hat{d}_m^\dagger \hat{c}_k + H.c.) \\ \hat{V}_{SP} &= \sum_{m_1, m_2} \sum_{\alpha \in P} V_{m_1 m_2}^\alpha (\hat{b}_{m_1 m_2} + \hat{b}_{m_1 m_2}^\dagger) (\hat{a}_\alpha + \hat{a}_\alpha^\dagger) \end{aligned} \quad (12)$$

describe electron transfer between the system and contact L (R) and describes coupling to phonon α in the thermal bath P , respectively. Here, \hat{d}_m^\dagger (\hat{d}_m) and \hat{c}_k^\dagger (\hat{c}_k) creates (annihilates) electron in orbital m on the system and in state k of the contacts, respectively, \hat{a}_α^\dagger (\hat{a}_α) creates annihilates phonon in mode α , and $\hat{b}_{m_1 m_2} = \hat{d}_{m_1}^\dagger \hat{d}_{m_2}$.

For the system Hamiltonian we consider resonant level (RLM),

$$\hat{H}_S = \varepsilon_0 \hat{n}, \quad (13)$$

and Anderson impurity (AIM),

$$\hat{H}_S = \sum_{m=1,2} \varepsilon_0 \hat{n}_m + U \hat{n}_1 \hat{n}_2, \quad (14)$$

models. Here, $\hat{n}_m = \hat{d}_m^\dagger \hat{d}_m$ and U is the Coulomb repulsion. In the AIM two types of coupling to the thermal bath are considered: symmetric, $V_{m_1 m_2}^\alpha = \delta_{m_1, m_2} V_{m_1}^\alpha$, and anti-symmetric, $V_{m_1 m_2}^\alpha = \delta_{m_1, m_2} (-1)^{m_1} V_{m_1}^\alpha$.

Using Eq. (8) we calculate single- and two-particle GFs and employ them to evaluate the spectral functions $A_m(E)$, electron current⁵², I_L , at the left interface and phonon energy flux¹⁵, J_P , out of the system

$$\begin{aligned} A_m(E) &= -\frac{1}{\pi} \text{Im} G_{mm}^r(E) \\ I_L = -I_R &= \int \frac{dE}{2\pi} \text{Tr} [\Sigma_L^<(E) G^>(E) - \Sigma_L^>(E) G^<(E)] \\ J_P &= \int \frac{dE}{2\pi} E \text{Tr} [\Pi_P^<(E) D^>(E) - \Pi_P^>(E) D^<(E)] \end{aligned} \quad (15)$$

at steady-state. Here, $<$, $>$ and r are respectively lesser, greater and retarded projections of the GFs, self-energies Σ and Π are defined in Eq.(3), and trace is over molecular orbitals. in expression for $I_{L(R)}$ and over intra-molecular transitions in expression for J_P .

Reference system for both models utilizes three auxiliary sites: two mediating coupling of the physical site to full and empty Fermi baths and one two-level system

mediating coupling between physical site and empty Bose bath (see Fig. 1b and Appendix B). As mentioned earlier bigger sizes of auxiliary system require implementation of advanced methods (e.g., based on MPS) to solve auxiliary QME. Here, we restrict our consideration to small sizes which can be evaluated by direct diagonalization of the Liouvillian. We note that while for such small size representation of physical hybridization function in the auxiliary system is of limited quality (see Fig. 6), the aux-DB superperturbation expansion in the difference of the two hybridization function allows to obtain high quality results even for small reference system sizes.

B. Numerical results

We start from consideration of RLM studied within numerically exact QMC approach in Ref. 53. Parameters (in arbitrary energy units E_0) are $k_B T = 0.2$ and $\varepsilon_0 = 3.2$. Following Ref. 53 Fermi baths are treated within the wide-band approximation (WBA) with a soft cut-off: $\Gamma_{L/R}(E) = \Gamma_{L/R}/[1 + e^{\nu(E-E_C)}][1 + e^{-\nu(E-E_C)}]$ with

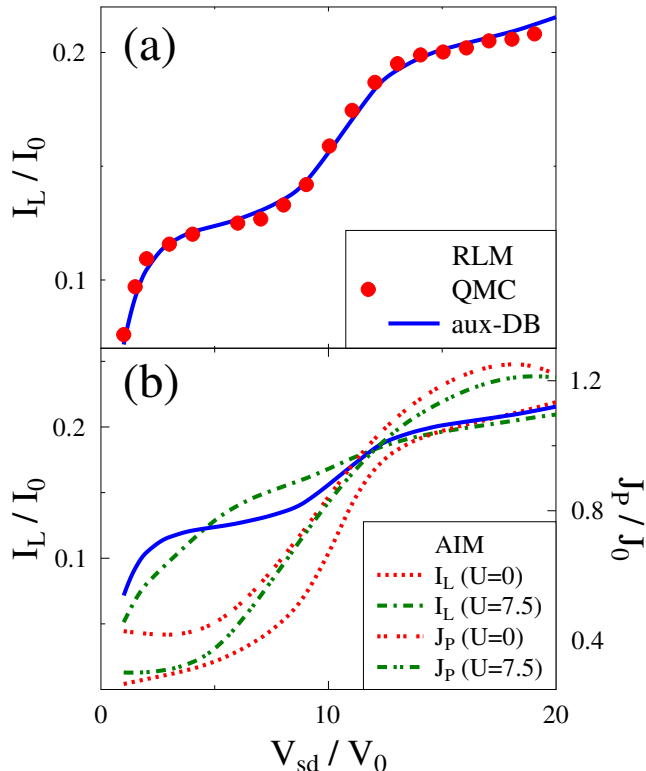


FIG. 2: (Color online) Electron I_L and phonon I_P fluxes. Shown are results for (a) RLM and (b) AIM. In panel (a) aux-DB results (solid line, blue) are benchmarked vs. numerically exact QMC calculation of Ref. 53. Panel (b) compares aux-DB results for AIM with $U = 0$ and $U = 7.5$. Solid line (blue) presents RLM simulations within aux-DB and is the same in both panels.

$\nu = 5$, $E_C = 20$ and $\Gamma_L = \Gamma_R = 0.5$; Bose bath is characterized by spectral density $J(\omega) = \gamma\omega/([\omega/\omega_0]^2 - 1)^2 + [\gamma\omega_0/(2M_0^2)]^2$ with $\gamma = 0.1$, $\omega_0 = 5$ and $M_0 = 4$. Bias was applied symmetrically: $\mu_L = -\mu_R = V/2$. Results of simulation are presented in terms of units of bias $V_0 = E_0/|e|$, flux $I_0 = E_0/\hbar$, and energy flux $J_0 = E_0^2/\hbar$. Fig. 2a compares aux-DB results (solid line) with numerically exact QMC (circles) simulations of Ref. 53.

Aux-DB simulations of the AIM with symmetric coupling to Bose bath for $U = 0$ (dotted line) and $U = 7.5$ (dashed line) Coulomb interaction are shown in Fig. 2b. Note that even in the absence of Coulomb interaction results of simulations are significantly different from results of the RLM (compare dotted and solid lines). This is due to effective electron-electron interaction induced by coupling to common Bose bath and the effect can be understood within an effective negative-U model ($\tilde{\varepsilon}_0 = \varepsilon_0 - M_0^2/\omega_0$ and $\tilde{U} = U - 2M_0^2/\omega_0$) which predicts doubly populated state $E_2 = 2\tilde{\varepsilon}_0 + \tilde{U} = -6.4$ to be the ground state of $U = 0$ quantum dot with energy gap of 6 to its singly populated state $E_1 = \tilde{\varepsilon}_0 = 0$. This shows that use of spinless models in studies of inelastic transport should be done with caution. For $U = 7.5$ (dash-dotted line) no current blockade is observed because electron transition from ground state is gapless. It is interesting to note that in blockaded region energy (phonon) flux is higher than for resonant tunneling (compare double-dotted and dash-double-dotted lines in Fig. 2b), which indicates predominantly elastic character of resonant transport.

Fig. 3 shows spectral functions simulated within the QME (dotted line), zero (dashed line), and first (solid line) aux-DB approaches for the cases of (a) symmetric and (b) anti-symmetric couplings to thermal bath. Fig. 3a shows results for AIM with $U = 0$, $M_0 = 4$ and symmetric coupling at $V_{sd} = 6$. Corresponding RLM results are given in the inset. While in RLM aux-DB is accurate already in the zero order, AIM $U = 0$ results are significantly renormalized when vertex corrections are taken into account. Fig. 3b shows results for AIM with $k_B T = 0$, $U = 5$ and $\varepsilon_0 = -U/2$, $M_0 = 0.1$ and anti-symmetric coupling at zero bias. One sees, that also in this case vertex corrections are important: they are necessary to reproduce Kondo feature.

Fig. 4a shows that Kondo is destroyed when increasing coupling strength M_0 to the thermal bath (compare dotted and dashed lines). The effect is due to the bath induced dephasing. Nonequilibrium simulation (solid line) shows the Kondo feature splitting. Finally, in Fig. 4b we show increase of Coulomb peaks broadening with increase of the coupling M_0 . Here parameters are $k_B T = 0$, $U = 5$ and $\varepsilon_0 = -U/2$, so that particle-hole symmetry is fulfilled. As previously, Fermi baths are considered within the WBA with $\nu = 10$ and $E_C = 20$. Bose bath is taken to be Ohmic: $J(\omega) = M_0 \omega e^{-\omega/\omega_C}$ with $\omega_C = 20$. To facilitate comparison peaks are shifted and scaled so that their maxima coincide and are equal to 1.

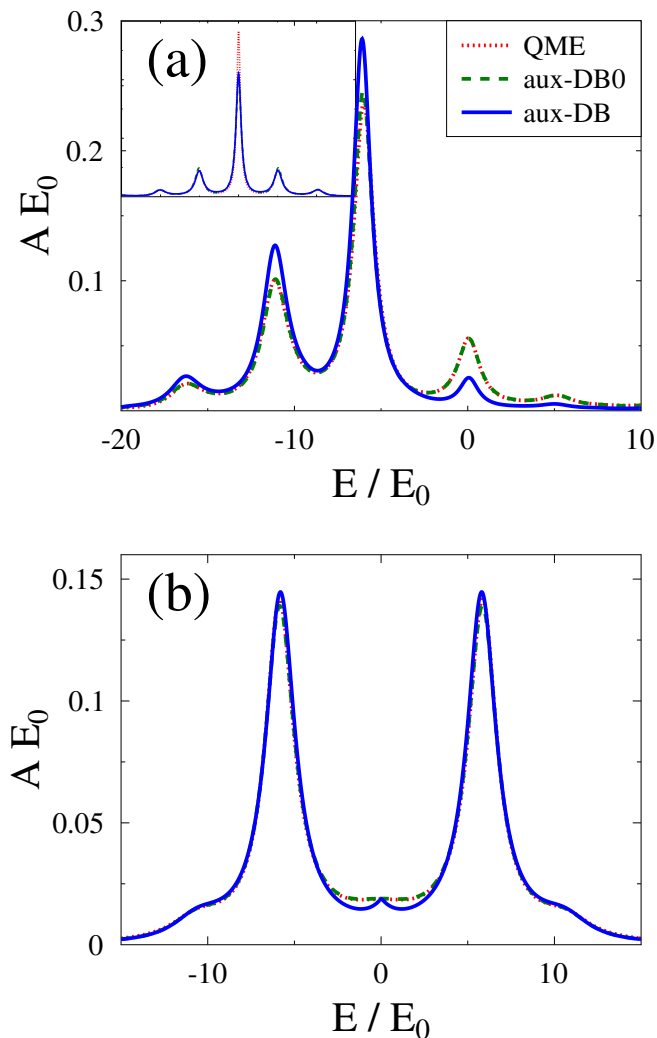


FIG. 3: (Color online) Spectral function A for AIM with (a) symmetric ($U = 0, V_{sd} = 6$) and (b) anti-symmetric ($U = 5, V_{sd} = 0$) couplings to the thermal bath P . Shown are results of the auxiliary QME (dotted line, red), zero (dashed line, green), and first order (solid line, blue) aux-DB approaches. Inset in (a) shows aux-DB results for RLM.

V. CONCLUSION

The nonequilibrium DF approach introduced originally in Ref. 26 and its optimization for steady-state simulations - the aux-DF approach²⁷ - are promising methods for modeling strongly correlated open systems. Contrary to usual diagrammatic expansions the methods can treat systems with no small parameter available. This is the situation often encountered in single-molecule optoelectronic devices, which are at the forefront of experimental and theoretical research due to interesting fundamental problems and applicational perspectives in energy nanomaterials, spintronics, and quantum computation. However, application of the aux-DF to simulations of optoelectronic devices is hindered by its inability to account

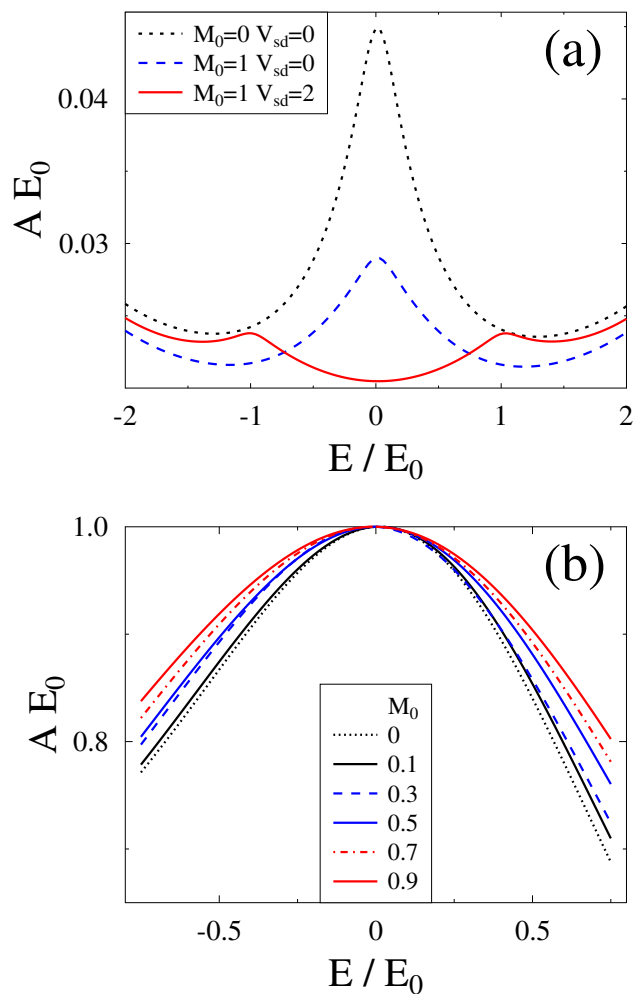


FIG. 4: (Color online) Spectral function A of AIM with anti-symmetric coupling to thermal bath P . Shown are results for several molecule-thermal bath coupling strengths (a) destruction of the Kondo peak by dephasing induced by coupling to thermal bath and (b) broadening of the Coulomb peaks (for comparison all Coulomb peaks are shifted to common maximum set at $E = 0$).

for energy exchange between molecule and plasmonic field. The latter is crucial in modeling of the devices.

Here we proposed a new nonequilibrium method, *the aux-DB approach*, which accounts for both electron and energy fluxes between system and baths. The nonequilibrium aux-DB is a super-perturbation theory inspired by equilibrium DB method³² proposed as generalization of the extended DMFT. Employing auxiliary QME and choosing infinite reference system makes the approach advantageous in treating the steady-states.

We utilized generic junction models of a molecule coupled to two Fermi leads and Bose phonon bath. The aux-DB was benchmarked vs. numerically exact QMC results of Ref. 53. We showed that the new scheme is both accurate and relatively numerically inexpensive. Further development of the method and its application to realis-

tic systems is a goal for future research.

Acknowledgments

M.G. acknowledges support by the National Science Foundation (grant CHE-1565939). The work of M.I.K. is supported by European Research Council via Synergy Grant 854843 - FASTCORR

Appendix A: Derivation of dual boson EOMs

Here we present derivation of the expressions for the zero order GFs, G_0^{DF} and D_0^{DB} , and self-energies, Σ^{DF} and Π^{DB} , for the dual boson technique, Eq. (6) of the main text.

We consider a physical system which consists from the molecule (d) coupled to Fermi (c) and Bose (a) baths. Its partition function on the Keldysh contour is⁴⁰

$$Z = \int_c D[\bar{d}, d, \bar{c}, c, \bar{a}, a] e^{iS[\bar{d}, d, \bar{c}, c, \bar{a}, a]} \quad (\text{A1})$$

where

$$\begin{aligned} S[\bar{d}, d, \bar{c}, c, \bar{a}, a] &= \bar{d}_1 [G_0^{-1}]_{12} d_2 + S^{int}[\bar{d}, d] \\ &+ \bar{c}_1 [g_B^{-1}]_{12} c_2 + \bar{a}_1 [d_B^{-1}]_{12} a_2 \\ &+ \bar{d}_1 V_{12} c_2 + \bar{c}_2 V_{21} d_1 + \bar{b}_1 V_{12} a_2 + \bar{a}_2 V_{21} b_1 \end{aligned} \quad (\text{A2})$$

is the action of an interacting system (molecule) coupled to non-interacting contacts (Fermi bath) and plasmon (Bose bath). Here, G_0^{-1} is defined in Eq. (2) of the main text and g_B^{-1} and d_B^{-1} are the inverse GFs for free electrons in the contacts and free photons in the Bose bath

$$\begin{aligned} [g_B^{-1}]_{12} &= \delta(\tau_1, \tau_2) [i\partial_{\tau_1} - \varepsilon_k] \\ [d_B^{-1}]_{12} &= \delta(\tau_1, \tau_2) [i\partial_{\tau_1} - \omega_\alpha] \end{aligned} \quad (\text{A3})$$

After integrating out baths degrees of freedom⁴¹ one gets effective action presented in Eq. (1) of the main text.

Next we introduce *an exactly solvable reference system*, which is identical to the original one in all intra-system interactions but differs from it by its hybridization function. Effective action of the original system will be related to that of the reference system via Eq. (4) of the main text. Because direct application of perturbation theory to Eq. (4) is not possible, we apply two Hubbard-Stratonovich transformations to introduce new particles, *dual fermion* (f) and *dual boson* (η), which disentangle last two terms in Eq. (4). Following Ref. 33 we get

$$\begin{aligned} e^{\bar{d}_1 N_{12} d_2} &= \\ Z_f \int_c D[\bar{f}, f] e^{-\bar{f}_1 \alpha_{12}^f [N^{-1}]_{23} \alpha_{34}^f f_4 + \bar{f}_1 \alpha_{12}^f d_2 + \bar{d}_1 \alpha_{12}^f f_2} \\ e^{\bar{b}_1 M_{12} b_2} &= \\ Z_b \int_c D[\bar{\eta}, \eta] e^{-\bar{\eta}_1 \alpha_{12}^b [M^{-1}]_{23} \alpha_{34}^b \eta_4 + \bar{\eta}_1 \alpha_{12}^b b_2 + \bar{b}_1 \alpha_{12}^b \eta_2} \end{aligned} \quad (\text{A4})$$

with

$$\begin{aligned} \alpha^f &= i g^{-1} & N &= i \delta \Sigma^B & Z_f &= (\det [\alpha^f N^{-1} \alpha^f])^{-1} \\ \alpha^b &= i \chi^{-1} & M &= i \delta \Pi^B & Z_b &= \det [\alpha^b M^{-1} \alpha^b] \end{aligned} \quad (\text{A5})$$

Applying the transformation to the partition function (A1) with the action given by Eq. (4) of the main text yields

$$Z = Z_f Z_b \int_c D[\bar{d}, d, \bar{f}, f, \bar{\eta}, \eta] e^{iS[\bar{d}, d, \bar{f}, f, \bar{\eta}, \eta]} \quad (\text{A6})$$

where

$$\begin{aligned} S[\bar{d}, d, \bar{f}, f, \bar{\eta}, \eta] &= \tilde{S}[d^*, d] \\ &- \bar{f}_1 g_{12}^{-1} [\delta \Sigma^B]_{23}^{-1} g_{34}^{-1} f_4 + \bar{f}_1 g_{12}^{-1} d_2 + \bar{d}_1 g_{12}^{-1} f_2 \\ &- \bar{\eta}_1 \chi_{12}^{-1} [\delta \Pi^B]_{23}^{-1} \chi_{34}^{-1} \eta_4 + \bar{\eta}_1 \chi_{12}^{-1} b_2 + \bar{b}_1 \chi_{12}^{-1} \eta_2 \end{aligned} \quad (\text{A7})$$

Thus, auxiliary quasi-particles - dual fermion (f) and dual boson (η) - were introduced.

Integrating out of the real quasiparticle, \bar{d} and d , in (A6) leads to

$$Z = Z_f Z_b \tilde{Z} \int_c D[\bar{f}, f, \bar{\eta}, \eta] e^{iS[\bar{f}, f, \bar{\eta}, \eta]} \quad (\text{A8})$$

with

$$\begin{aligned} S[\bar{f}, f, \bar{\eta}, \eta] &= \bar{f}_1 [G_0^{DF}]_{12}^{-1} f_2 + \bar{\eta}_1 [D_0^{DB}]_{12}^{-1} \eta_2 \\ &+ V[\bar{f}, f, \bar{\eta}, \eta] \end{aligned} \quad (\text{A9})$$

$[G_0^{DF}]_{12}^{-1}$ and $[D_0^{DB}]_{12}^{-1}$ are defined in Eq. (6) of the main text, \tilde{Z} is the partition function of the reference system, and $V[\bar{f}, f, \bar{\eta}, \eta]$ is unknown interaction between dual particles.

To get the interaction $V[\bar{f}, f, \bar{\eta}, \eta]$ we expand (A6) in $f-d$ and $\eta-b$ interactions and integrate out real quasi-particles, \bar{d} and d . Taking g and χ to be single electron and single molecular excitaton GFs of the reference system

$$\begin{aligned} g_{12} &= \frac{-i}{\tilde{Z}} \int_c D[\bar{d}, d] d_1 \bar{d}_2 e^{i\tilde{S}[\bar{d}, d]} \equiv -i \langle T_c \hat{d}_1 \hat{d}_2^\dagger \rangle_{ref} \\ \chi_{12} &= \frac{-i}{\tilde{Z}} \int_c D[\bar{d}, d] \delta b_1 \delta \bar{b}_2 e^{i\tilde{S}[\bar{d}, d]} \equiv -i \langle T_c \hat{b}_1 \hat{b}_2^\dagger \rangle_{ref} \end{aligned} \quad (\text{A10})$$

and comparing the resulting expression to expansion of (A8) yields expression for $V[\bar{f}, f, \bar{\eta}, \eta]$. In particular, for expansion up to fourth order in f , f and second order in $\bar{\eta}$, η

$$\begin{aligned} V[\bar{f}, f, \bar{\eta}, \eta] &= \bar{\eta}_1 \chi_{12}^{-1} \langle b_2 \rangle_{ref} + \langle \bar{b}_1 \rangle_{ref} \chi_{12}^{-1} \eta_2 \\ &- \frac{i}{4} \bar{f}_1 \bar{f}_3 \Gamma_{13;24} f_2 f_4 \\ &- \bar{\eta}_1 \gamma_{123} \bar{f}_2 f_3 - \bar{f}_3 f_2 \delta_{321} \eta_1 \end{aligned} \quad (\text{A11})$$

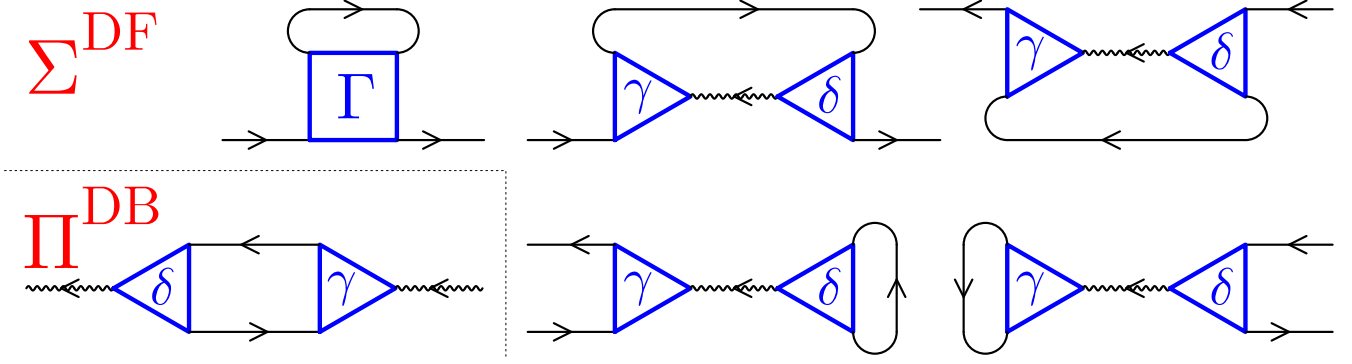


FIG. 5: Contributions to diagrams for dual fermion, Σ^{DF} , and dual boson, Π^{DB} , self-energies, Eq. (6). Directed solid and wavy lines (black) indicate dual fermion and dual boson GFs, G_0^{DF} and D_0^{DB} , respectively. Triangle and square (blue) indicate vertices γ and Γ of the reference system.

Here γ_{123} , δ_{321} and $\Gamma_{13;24}$ are vertices of the reference system

$$\begin{aligned} \Gamma_{13;24} &= g_{11'}^{-1} g_{33'}^{-1} \left[-\langle T_c \hat{d}_{1'} \hat{d}_{2'}^\dagger \hat{d}_{3'} \hat{d}_{4'}^\dagger \rangle_{ref} \right. \\ &\quad \left. - g_{1'2'} g_{3'4'} + g_{1'4'} g_{3'2'} \right] g_{2'2}^{-1} g_{4'4}^{-1} \\ \gamma_{123} &= \chi_{11'}^{-1} g_{22'}^{-1} \langle T_c \delta \hat{b}_{1'} \hat{d}_{2'} \hat{d}_{3'}^\dagger \rangle_{ref} g_{3'3}^{-1} \\ \delta_{321} &= g_{33'}^{-1} \langle T_c \hat{d}_{3'} \hat{d}_{2'}^\dagger \delta \hat{b}_{1'} \rangle_{ref} \chi_{1'1}^{-1} g_{2'2}^{-1} \end{aligned} \quad (\text{A12})$$

Here T_c is contour ordering operator, subscript *ref* indicates Markov Lindblad-type evolution of the reference system and $\delta \hat{b} \equiv \hat{b} - \langle \hat{b} \rangle_{ref}$. We note in passing that projections of the vertices γ_{123} and δ_{321} are related via

$$[\gamma_{123}^{s_1 s_2 s_3}]^* = -\delta_{321}^{\bar{s}_3 \bar{s}_2 \bar{s}_1} \quad (\text{A13})$$

where $s_{1,2,3} \in \{-, +\}$ indicate branches of the Keldysh contour and \bar{s} is the branch opposite to s .

Finally, using (A8) with interaction given by (A11) in expansion of GFs for the dual particles

$$\begin{aligned} G_{12} &\equiv -i \langle T_c f_1 \bar{f}_2 \rangle \\ D_{12} &\equiv -i \langle T_c b_1 \bar{b}_2 \rangle \end{aligned} \quad (\text{A14})$$

up to second order and employing the Wick's theorem yields the dual particles self-energies given in Eq. (6) of the main text. Corresponding diagrams are shown in Fig. 5.

Appendix B: Fitting hybridization functions with auxiliary modes

Recently, exact proof of possibility to map unitary evolution of a physical system onto Markov Lindblad-type evolution of an auxiliary system was established for systems interacting with Fermi⁴⁸⁻⁵¹ and Bose^{46,47} baths. At the heart of the mapping is fitting of hybridization functions of the physical system with set of auxiliary modes in the auxiliary system. Here, we give details of the fitting procedure.

Explicit form for the Markov Lindblad-type QME (9) is

$$\frac{d\rho^{SA}(t)}{dt} = -i\mathcal{L}\rho^{SA}(t) \equiv -i[\hat{H}_{SA}, \rho^{SA}(t)] + \mathcal{D}\rho^{SA}(t) \quad (\text{B1})$$

with the Liouvillian taken as

$$\begin{aligned} \hat{H}_{SA} &= \hat{H}_S + \sum_{n_1, n_2} \epsilon_{m_1 m_2} \hat{c}_{n_1}^\dagger \hat{c}_{n_2} \\ &+ \sum_{m, n} (t_{mn} \hat{d}_m^\dagger \hat{c}_n + t_{mn}^* \hat{c}_n^\dagger \hat{d}_m) \\ &+ \sum_{\beta_1, \beta_2} \omega_{\beta_1 \beta_2} \hat{e}_{\beta_1}^\dagger \hat{e}_{\beta_2} \\ &+ \sum_{m_1, m_2, \beta} r_{m_1 m_2}^\beta (\hat{b}_{m_1 m_2}^\dagger + \hat{b}_{m_1 m_2}^\dagger) (\hat{e}_\beta + \hat{e}_\beta^\dagger) \end{aligned} \quad (\text{B2})$$

$$\begin{aligned} \mathcal{D}\rho &= \sum_{n_1, n_2} \left(\Gamma_{n_1 n_2}^{(R)} (\hat{c}_{n_2} \hat{\rho} \hat{c}_{n_1}^\dagger - \frac{1}{2} \{ \hat{\rho}, \hat{c}_{n_1}^\dagger \hat{c}_{n_2} \}) \right. \\ &\quad \left. + \Gamma_{n_1 n_2}^{(L)} (\hat{c}_{n_1}^\dagger \hat{\rho} \hat{c}_{n_2} - \frac{1}{2} \{ \hat{\rho}, \hat{c}_{n_2} \hat{c}_{n_1}^\dagger \}) \right) \\ &+ \sum_{\beta_1, \beta_2} \gamma_{\beta_1 \beta_2}^{(P)} (\hat{e}_{\beta_2} \hat{\rho} \hat{e}_{\beta_1}^\dagger - \frac{1}{2} \{ \hat{e}_{\beta_1}^\dagger \hat{e}_{\beta_2}, \hat{\rho} \}) \end{aligned}$$

Here \hat{c}_n^\dagger (\hat{c}_n) and \hat{e}_β^\dagger (\hat{e}_β) create (annihilate) excitation in auxiliary Fermi mode n and Bose mode β , respectively.

Following Refs. 49,51 we construct retarded, $\tilde{\Sigma}^r$, and Keldysh, $\tilde{\Sigma}^K$, projections of the Fermi hybridization function in the auxiliary system as

$$\begin{aligned} \tilde{\Sigma}_{m_1 m_2}^r(E) &= \sum_{n_1, n_2} t_{m_1 n_1} \tilde{G}_{n_1 n_2}^r(E) t_{m_2 n_2}^* \\ \tilde{\Sigma}_{m_1 m_2}^K(E) &= \sum_{n_1, n_2} t_{m_1 n_1} \tilde{G}_{n_1 n_2}^K(E) t_{m_2 n_2}^* \end{aligned} \quad (\text{B3})$$

where

$$\begin{aligned} \tilde{G}^r(E) &= \left(E \mathbf{I} - \epsilon + \frac{i}{2} (\mathbf{\Gamma}^{(R)} + \mathbf{\Gamma}^{(L)}) \right)^{-1} \\ \tilde{G}^K(E) &= i \tilde{G}^r(E) (\mathbf{\Gamma}^{(L)} - \mathbf{\Gamma}^{(R)}) \tilde{G}^a(E) \end{aligned} \quad (\text{B4})$$

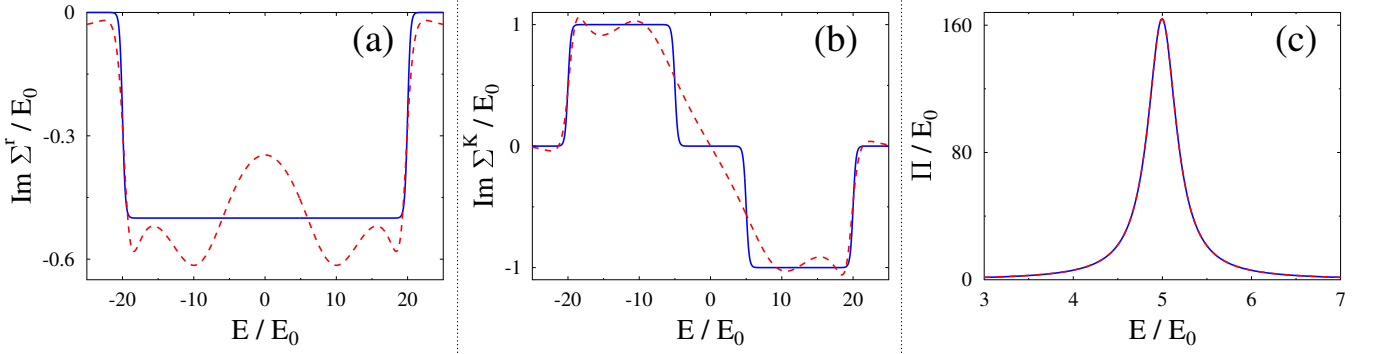


FIG. 6: Hybridization functions of the physical (solid line, blue) and auxiliary (dashed line, red) systems. Shown are (a) retarded and (b) Keldysh projections of the self-energy due to coupling to contacts and (c) hybridization function due to coupling to thermal bath. Fitting is done for parameters adopted in the first numerical example presented in the main text.

are retarded, $\tilde{\mathbf{G}}^r(E)$, and Keldysh, $\tilde{\mathbf{G}}^K(E)$ projections of the Fermi auxiliary modes Green's functions, and where $\tilde{\mathbf{G}}^a(E) \equiv [\tilde{\mathbf{G}}^r(E)]^\dagger$ is its advanced projection. Hybridization functions (B3) should fit corresponding hybridization functions

$$\begin{aligned}\Sigma_{m_1 m_2}^r(E) &= \sum_{k \in \{L, R\}} V_{m_1 k} g_k^r(E) V_{k m_2} \\ \Sigma_{m_1 m_2}^K(E) &= \sum_{k \in \{L, R\}} V_{m_1 k} g_k^K(E) V_{k m_2}\end{aligned}\quad (\text{B5})$$

of the physical system. Here

$$\begin{aligned}g_k^r(E) &\equiv (E - \varepsilon_k + i\delta)^{-1} \\ g_k^K(E) &\equiv 2\pi i (2n_k - 1) \delta(E - \varepsilon_k)\end{aligned}\quad (\text{B6})$$

are the retarded and Keldysh projections of the free electron in state k in contacts, n_k is the Fermi-Dirac thermal distribution and $\delta = 0^+$

We construct Bose hybridization function in the auxiliary system following Refs. 46,47. For the physical system-bosonic bath coupling taken in the form

$$\sum_{m_1 m_2} \sum_{\alpha} V_{m_1 m_2}^{\alpha} (\hat{b}_{m_1 m_2} + \hat{b}_{m_1 m_2}^{\dagger}) (\hat{a}_{\alpha} + \hat{a}_{\alpha}^{\dagger}) \quad (\text{B7})$$

the effect of the bosonic environment can be fully encoded by correlation function

$$\begin{aligned}\Pi_{m_1 m_2, m_3 m_4}(t - t') &= \\ \sum_{\alpha} V_{m_1 m_2}^{\alpha} \langle (\hat{a}_{\alpha} + \hat{a}_{\alpha}^{\dagger})(t) (\hat{a}_{\alpha} + \hat{a}_{\alpha}^{\dagger})(t') \rangle V_{m_3 m_4}^{\alpha}\end{aligned}\quad (\text{B8})$$

Similarly, coupling to auxiliary Bose modes in (B2) is fully described by correlation function

$$\begin{aligned}\tilde{\Pi}_{m_1 m_2, m_3 m_4}(t - t') &= \\ \sum_{\beta_1, \beta_2} r_{m_1 m_2}^{\beta_1} \langle (\hat{e}_{\beta_1} + \hat{e}_{\beta_1}^{\dagger})(t) (\hat{e}_{\beta_2} + \hat{e}_{\beta_2}^{\dagger})(t') \rangle r_{m_3 m_4}^{\beta_2} \\ \equiv i \sum_{\beta_1, \beta_2} r_{m_1 m_2}^{\beta_1} (\tilde{D}_{\beta_1 \beta_2}^>(t - t') + \tilde{D}_{\beta_2 \beta_1}^<(t' - t))\end{aligned}\quad (\text{B9})$$

Here $\tilde{D}^>$ and $\tilde{D}^<$ are the greater and lesser projections of Bose auxiliary mode Green's function

$$\tilde{D}_{\beta_1 \beta_2}(\tau_1, \tau_2) = -i \langle T_c \hat{e}_{\beta_1}(\tau_1) \hat{e}_{\beta_2}^{\dagger}(\tau_2) \rangle \quad (\text{B10})$$

Fourier transform of the correlation function (B9) is

$$\tilde{\Pi}_{m_1 m_2, m_3 m_4}(E) = i \sum_{\beta_1, \beta_2} r_{m_1 m_2}^{\beta_1} (\tilde{D}_{\beta_1 \beta_2}^>(E) + \tilde{D}_{\beta_2 \beta_1}^<(-E)) \quad (\text{B11})$$

According to Ref. 46 in auxiliary system one considers Bose bath at zero temperature with eigenmodes spanning energy range from $-\infty$ to $+\infty$. Thus, greater and lesser projections of the Green's function (B10) satisfy

$$\begin{aligned}\tilde{\mathbf{D}}^>(E) &= -i \tilde{\mathbf{D}}^r(E) \gamma^{(P)} \tilde{\mathbf{D}}^a(E) \\ \tilde{\mathbf{D}}^<(E) &= 0\end{aligned}\quad (\text{B12})$$

where

$$\begin{aligned}\tilde{\mathbf{D}}^r(E) &= (E I - \omega + \frac{i}{2} \gamma^{(P)})^{-1} \\ \tilde{\mathbf{D}}^a(E) &= [\tilde{\mathbf{D}}^r(E)]^{\dagger}\end{aligned}\quad (\text{B13})$$

are the retarded projection and advanced projections.

For the correlation function (B8) representing physical system and for the case of thermal Bose bath with inverse temperature β

$$\begin{aligned}\Pi_{m_1 m_2, m_3 m_4}(E) &= \left(1 + \coth \frac{\beta E}{2}\right) \\ &\times \left(J_{m_1 m_2, m_3 m_4}(E) \theta(E) - J_{m_3 m_4, m_1 m_2}(-E) \theta(-E)\right)\end{aligned}\quad (\text{B14})$$

where

$$J_{m_1 m_2, m_3 m_4}(E) \equiv \pi \sum_{\alpha} V_{m_1 m_2}^{\alpha} V_{m_3 m_4}^{\alpha} \delta(E - \omega_{\alpha}) \quad (\text{B15})$$

Following Ref. 47 we stress that although the auxiliary Bose bath is taken at zero temperature this does not restrict the temperature of Bose bath in the physical system: the information about finite temperature will be provided by parameters of the auxiliary Bose modes.

Finally note that parameters $\epsilon_{m_1 m_2}$, t_{mn} , $\omega_{\beta_1 \beta_2}$, $r_{m_1 m_2}^\beta$, $\Gamma_{n_1 n_2}^{(L)}$, $\Gamma_{n_1 n_2}^{(R)}$ and $\gamma_{\beta_1 \beta_2}^{(P)}$ of the Lindblad equation (B1)-(B2) are used to fit hybridization functions (B5) and (B14) of the physical system with corresponding hybridization functions (B3) and (B11) of the auxiliary model employing a cost function to quantify deviation⁵¹. Figure 6 shows hybridization functions for the physical model (solid lines) and their fitting with auxiliary modes (dashed lines) as utilized in simulations of the RLM and AIM with symmetric coupling to thermal bath presented in the main text. We used four Fermi and one Bose auxiliary modes to fit the corresponding hybridization functions.

Appendix C: Green's Functions and vertices of the reference system

To evaluate dual-particles self-energies, Eq. (6) of the main text, one has to calculate GFs g and χ , Eq. (A10), and vertices γ , δ and Γ , Eq. (A12), of the reference system. These quantities are given by two- (g and χ), three- (γ , δ) and four-time (Γ) correlation functions defined on the Keldysh contour.

To provide these we utilize the quantum regression relation

Because Markov Lindblad-type QME is used to solve the reference system, we can employ the quantum regression relation⁵⁴

$$\langle T_c \hat{A}(\tau_1) \hat{B}(\tau_2) \dots \hat{Z}(\tau_n) \rangle = \text{Tr}[\mathcal{O}_n \mathcal{U}(t_n, t_{n-1}) \dots \mathcal{O}_2 \mathcal{U}(t_2, t_1) \mathcal{O}_1 \mathcal{U}(t_1, 0) \rho^{SA}(0)] \quad (\text{C1})$$

to evaluate correlation functions. Here $\rho^{SA}(0)$ is the steady-state density matrix of the extended system, $\mathcal{U}(t_i, t_{i-1})$ is the Liouville space evolution operator and times t_i are ordered so that $t_n > t_{n-1} > \dots > t_2 > t_1 > 0$. \mathcal{O}_i is the Liouville space super-operator corresponding to one of operators $\hat{A} \dots \hat{Z}$ whose time is i -th in the ordering. It acts from the left (right) for the operator on the forward (backward) branch of the contour. The steady-state density matrix is found as a right eigenvector $|R_0\rangle \gg$ corresponding to the Liouvillian eigenvalue $\lambda_0 = 0$. Using spectral decomposition of the Liouvillian, the evolution operator can be presented in its eigenbasis as

$$\mathcal{U}(t_i, t_{i-1}) = \sum_{\gamma} |R_{\gamma}\rangle \gg e^{-i\lambda_{\gamma}(t_i - t_{i-1})} \ll L_{\gamma}|. \quad (\text{C2})$$

For evaluation of single- and two-particle GFs, besides the \mathcal{L} of Eq. (9) of the main text we will also need Liouvillians $\mathcal{L}^{(\pm 1)}$ and $\mathcal{L}^{(\pm 2)}$. These are evolution operator generators for Liouville space vectors $|S_1 S_2\rangle \gg$ with different number N_S of electrons in states $|S_1\rangle$ and $|S_2\rangle$: $N_{S_1} - N_{S_2} = \pm 1, \pm 2$.

Using (C2) in (C1) yields expressions for the single-particle (g and χ) and two-particle GFs of the reference system (see Appendix C for details). To do so we have to consider several projections (contour orderings) and time orderings. In particular, evaluation of two-time correlation functions requires consideration of $2^1 = 2$ projections with $2! = 2$ time orderings for each projection. Three-time correlation functions will require consideration of $2^2 = 4$ projections with $3! = 6$ time orderings. Evaluation of four-time correlation function requires consideration of $2^3 = 8$ projections with $4! = 24$ time orderings. Evaluating projections one has to take care of sign of Fermi operators permutations.

$$\langle T_c \hat{O}_1(\tau_1) \hat{O}_2(\tau_2) \dots \hat{O}_N(\tau_N) \rangle_{ref} = (-1)^P \langle \langle I | \mathcal{O}_{\theta_1} \mathcal{U}(t_{\theta_1}, t_{\theta_2}) \mathcal{O}_{\theta_2} \mathcal{U}(t_{\theta_2}, t_{\theta_3}) \dots \dots \mathcal{O}_{\theta_N} \mathcal{U}(t_{\theta_N}, 0) | \rho^{SA}(0) \rangle \rangle \quad (\text{C3})$$

Here P is number of Fermi interchanges in the permutation of operators \hat{O}_i by T_c , $\langle \langle I |$ is the Liouville space bra representation of the Hilbert space identity operator, θ_i are indices of operators \hat{O}_i rearranged in such a way that $t_{\theta_1} > t_{\theta_2} > \dots > t_{\theta_N}$ (t_{θ_i} is real time corresponding to contour variable τ_{θ_i}), \mathcal{U} is the Liouville space evolution superoperator defined in Eq. (11), and \mathcal{O}_{θ_i} are the Liouville space superoperators corresponding to the Hilbert space operators \hat{O}_i

$$\mathcal{O}_i |\rho\rangle = \begin{cases} \mathcal{O}_i^- |\rho\rangle \equiv \hat{O}_i \hat{\rho} & \text{forward branch} \\ \mathcal{O}_i^+ |\rho\rangle \equiv \hat{\rho} \hat{O}_i & \text{backward branch} \end{cases} \quad (\text{C4})$$

Further details on evaluation of multi-time correlation functions can be found in Ref. 27.

Once single- and two-particle GFs of the reference system are known, the vertices required in Eq. (6) of the main text can be calculated from their definitions, Eq. (A12).

* Electronic address: fec011@ucsd.edu

† Electronic address: M.Katsnelson@science.ru.nl

‡ Electronic address: migalperin@ucsd.edu

¹ Z. Ioffe, T. Shamai, A. Ophir, G. Noy, I. Yutsis, K. Kfir, O. Cheshnovsky, and Y. Selzer, Nature Nanotech. **3**, 727 (2008).

² D. R. Ward, N. J. Halas, J. W. Ciszek, J. M. Tour, Y. Wu, P. Nordlander, and D. Natelson, Nano Lett. **8**, 919 (2008).

³ D. R. Ward, D. A. Corley, J. M. Tour, and D. Natelson, Nature Nanotech. **6**, 33 (2011).

⁴ Z. Liu, S.-Y. Ding, Z.-B. Chen, X. Wang, J.-H. Tian, J. R. Anema, X.-S. Zhou, D.-Y. Wu, B.-W. Mao, X. Xu, et al.,

- Nat. Commun. **2**, 305 (2011).
- ⁵ N. Chiang, N. Jiang, D. V. Chulhai, E. A. Pozzi, M. C. Hersam, L. Jensen, T. Seideman, and R. P. V. Duyne, Nano Lett. **15**, 4114 (2015).
 - ⁶ J. Lee, N. Tallarida, X. Chen, P. Liu, L. Jensen, and V. A. Apkarian, ACS Nano **11**, 11466 (2017).
 - ⁷ N. L. Schneider, J. T. Lü, M. Brandbyge, and R. Berndt, Phys. Rev. Lett. **109**, 186601 (2012).
 - ⁸ E. Čavar, M.-C. Blüm, M. Pivetta, F. Patthey, M. Chergui, and W.-D. Schneider, Phys. Rev. Lett. **95**, 196102 (2005).
 - ⁹ C. Chen, P. Chu, C. A. Bobisch, D. L. Mills, and W. Ho, Phys. Rev. Lett. **105**, 217402 (2010).
 - ¹⁰ Z. C. Dong, X. L. Zhang, H. Y. Gao, Y. Luo, C. Zhang, L. G. Chen, R. Zhang, X. Tao, Y. Zhang, J. L. Yang, et al., Nat. Photon. **4**, 50 (2010).
 - ¹¹ H. Imada, K. Miwa, M. Imai-Imada, S. Kawahara, K. Kimura, and Y. Kim, Nature **538**, 364 (2016), ISSN 1476-4687.
 - ¹² H. Imada, K. Miwa, M. Imai-Imada, S. Kawahara, K. Kimura, and Y. Kim, Phys. Rev. Lett. **119**, 013901 (2017).
 - ¹³ K. Kimura, K. Miwa, H. Imada, M. Imai-Imada, S. Kawahara, J. Takeya, M. Kawai, M. Galperin, and Y. Kim, Nature **570**, 210 (2019).
 - ¹⁴ M. Galperin and A. Nitzan, Phys. Chem. Chem. Phys. **14**, 9421 (2012).
 - ¹⁵ M. Galperin, Chem. Soc. Rev. **46**, 4000 (2017).
 - ¹⁶ J. Gersten and A. Nitzan, J. Chem. Phys. **73**, 3023 (1980).
 - ¹⁷ R. Chikkaraddy, B. de Nijs, F. Benz, S. J. Barrow, O. A. Scherman, E. Rosta, A. Demetriadou, P. Fox, O. Hess, and J. J. Baumberg, Nature **535**, 127 (2016).
 - ¹⁸ N. Kongsuwan, A. Demetriadou, R. Chikkaraddy, F. Benz, V. A. Turek, U. F. Keyser, J. J. Baumberg, and O. Hess, ACS Photonics **5**, 186 (2018).
 - ¹⁹ G. Cohen, E. Gull, D. R. Reichman, and A. J. Millis, Phys. Rev. Lett. **115**, 266802 (2015).
 - ²⁰ A. E. Antipov, Q. Dong, J. Kleinhenz, G. Cohen, and E. Gull, Phys. Rev. B **95**, 085144 (2017).
 - ²¹ M. Ridley, V. N. Singh, E. Gull, and G. Cohen, Phys. Rev. B **97**, 115109 (2018).
 - ²² F. B. Anders, Phys. Rev. Lett. **101**, 066804 (2008).
 - ²³ S. Schmitt and F. B. Anders, Phys. Rev. B **81**, 165106 (2010).
 - ²⁴ U. Schollwöck, Rev. Mod. Phys. **77**, 259 (2005).
 - ²⁵ U. Schollwöck, Annals of Physics **326**, 96 (2011).
 - ²⁶ C. Jung, A. Lieder, S. Brener, H. Hafermann, B. Baxevanis, A. Chudnovskiy, A. Rubtsov, M. Katsnelson, and A. Lichtenstein, Annalen der Physik **524**, 49 (2012).
 - ²⁷ F. Chen, G. Cohen, and M. Galperin, Phys. Rev. Lett. **122**, 186803 (2019).
 - ²⁸ A. N. Rubtsov, M. I. Katsnelson, and A. I. Lichtenstein, Phys. Rev. B **77**, 033101 (2008).
 - ²⁹ Hafermann, H., Jung, C., Brener, S., Katsnelson, M. I., Rubtsov, A. N., and Lichtenstein, A. I., EPL **85**, 27007 (2009).
 - ³⁰ A. E. Antipov, J. P. F. LeBlanc, and E. Gull, Physics Procedia **68**, 43 (2015).
 - ³¹ G. Rohringer, H. Hafermann, A. Toschi, A. A. Katanin, A. E. Antipov, M. I. Katsnelson, A. I. Lichtenstein, A. N. Rubtsov, and K. Held, Rev. Mod. Phys. **90**, 025003 (2018).
 - ³² A. Rubtsov, M. Katsnelson, and A. Lichtenstein, Ann. Phys. **327**, 1320 (2012).
 - ³³ E. G. C. P. van Loon, A. I. Lichtenstein, M. I. Katsnelson, O. Parcollet, and H. Hafermann, Phys. Rev. B **90**, 235135 (2014).
 - ³⁴ E. G. C. P. van Loon, H. Hafermann, A. I. Lichtenstein, A. N. Rubtsov, and M. I. Katsnelson, Phys. Rev. Lett. **113**, 246407 (2014).
 - ³⁵ E. G. C. P. van Loon, M. I. Katsnelson, and M. Lemeshko, Phys. Rev. B **92**, 081106(R) (2015).
 - ³⁶ E. A. Stepanov, E. G. C. P. van Loon, A. A. Katanin, A. I. Lichtenstein, M. I. Katsnelson, and A. N. Rubtsov, Phys. Rev. B **93**, 045107 (2016).
 - ³⁷ E. G. C. P. van Loon, F. Krien, H. Hafermann, E. A. Stepanov, A. I. Lichtenstein, and M. I. Katsnelson, Phys. Rev. B **93**, 155162 (2016).
 - ³⁸ E. A. Stepanov, A. Huber, E. G. C. P. van Loon, A. I. Lichtenstein, and M. I. Katsnelson, Phys. Rev. B **94**, 205110 (2016).
 - ³⁹ E. A. Stepanov, S. Brener, F. Krien, M. Harland, A. I. Lichtenstein, and M. I. Katsnelson, Phys. Rev. Lett. **121**, 037204 (2018).
 - ⁴⁰ A. Kamenev, *Field Theory of Non-Equilibrium Systems* (Cambridge University Press, 2011).
 - ⁴¹ J. W. Negele and H. Orland, *Quantum Many-Particle Systems*, vol. 68 (Addison-Wesley Publishing Company, Redwood City, California, 1988).
 - ⁴² M. Wagner, Phys. Rev. B **44**, 6104 (1991).
 - ⁴³ A. L. Fetter and J. D. Walecka, *Quantum Theory of Many-Particle Systems* (McGraw-Hill Book Company, 1971).
 - ⁴⁴ P. Coleman, *Introduction to Many-Body Physics* (Cambridge University Press, 2015).
 - ⁴⁵ G. Stefanucci and R. van Leeuwen, *Nonequilibrium Many-Body Theory of Quantum Systems. A Modern Introduction*. (Cambridge University Press, 2013).
 - ⁴⁶ D. Tamascelli, A. Smirne, S. F. Huelga, and M. B. Plenio, Phys. Rev. Lett. **120**, 030402 (2018).
 - ⁴⁷ F. Mascherpa, A. Smirne, D. Tamascelli, P. F. Acebal, S. Donadi, S. F. Huelga, and M. B. Plenio, arXiv:1904.04822 [quant-ph] (2019).
 - ⁴⁸ E. Arrigoni, M. Knap, and W. von der Linden, Phys. Rev. Lett. **110**, 086403 (2013).
 - ⁴⁹ A. Dorda, M. Ganahl, H. G. Evertz, W. von der Linden, and E. Arrigoni, Phys. Rev. B **92**, 125145 (2015).
 - ⁵⁰ A. Dorda, M. Sorantin, W. v. d. Linden, and E. Arrigoni, New J. Phys. **19**, 063005 (2017), ISSN 1367-2630.
 - ⁵¹ F. Chen, E. Arrigoni, and M. Galperin, arXiv:1909.08658 (2019).
 - ⁵² A.-P. Jauho, N. S. Wingreen, and Y. Meir, Phys. Rev. B **50**, 5528 (1994).
 - ⁵³ L. Mühlbacher and E. Rabani, Phys. Rev. Lett. **100**, 176403 (2008).
 - ⁵⁴ H.-P. Breuer and F. Petruccione, *The Theory of Open Quantum Systems* (Oxford University Press, 2003).